Acta Physica Universitatis Comenianae
Vol. L–LI, Number 1&2 (2009–2010) 85–93

Optical and Electrical Study of Transient Spark Discharge in Air*

M. Janda[1], Z. Machala[1], C. O. Laux[2]

[1]Division of Environmental Physics, Department of Astronomy, Earth Physics and Meteorology, Comenius University, Mlynská dolina, Bratislava 842 48, Slovakia
[2]Laboratoire E.M2.C CNRS-UPR288, Ecole Centrale Paris, Grande Voie des Vignes, 92295 Châtenay-Malabry, France

Abstract: We have investigated a novel type of streamer-to-spark transition discharge in air at atmospheric pressure named the transient spark (TS), applicable for flue gas cleaning or bio-decontamination. Despite the DC applied voltage, TS has a pulsed character with short (<100 ns) high current (>1 A) pulses, with repetitive frequencies of a few kHz. The emission of N_2 2^{nd} and 1^{st} positive, N_2^+ 1^{st} negative, and atomic N and O lines, was detected. The non-equilibrium character of TS was confirmed by calculated vibrational (3 000–5 000 K) and rotational (500–1 500 K) temperatures. Additionally, temporal emission profiles were obtained using PMT measurements.

1. Introduction

Atmospheric pressure plasmas in air generated by electrical discharges present a considerable interest for a wide range of environmental, bio-medical and industrial applications, such as air pollution control, waste water cleaning, bio-decontamination and sterilization, or material and surface treatment [1–6]. New types of discharges are therefore still being developed and studied, with a focus on efficiency, power requirements, stability, reliability and simplicity [7].

Besides measurements of electrical discharge parameters, optical emission spectroscopy (OES) in UV-VIS regions is widely used for plasma diagnostics. It provides valuable information on excited atomic and molecular states, enables to determine the rotational, vibrational, and electronic excitation temperatures of the plasma and thus the level of non-equilibrium and the gas temperature [8, 9]. In addition, it enables to identify many radicals and active atomic or molecular species and it so gives insight into the plasma chemical processes. This enables understanding and optimizing air or water pollution control processes [6].

2. Experimental Setup

Experiments were carried out at the room temperature in atmospheric pressure air with an axial flow of 10 l/min. The distance between stainless steel needle electrodes in point-to-point configuration varied from 3.5 to 5 mm. A DC High Voltage (HV) power supply HCL 14-20000 connected via a series resistor (R = 10 M) limiting the total

*) *Dedicated to Professor Peter Lukáč and Professor Viktor Martišovitš on the occasion of their 70th birthday.*

current was used to generate the positive TS discharge. The discharge voltage was measured by a high voltage probe LeCroy PMK-14kVAC and the discharge current was measured using the Pearson Electronics 2877 (1V/A) current probe linked to the 350 MHz digitizing oscilloscope LeCroy Waverunner 434 (maximum 2GS/s).

The UV-VIS spectra were obtained using a monochromator (Acton SpectraPro 2500i) fitted with an intensified CCD camera (Princeton Instruments PI-MAX). For time-resolved optical emission measurements, a photomultiplier tube (PMT) module with a 1.4-ns rise time (Hamamatsu H9305-3) was used in place of the monochromator. Its signal was recorded using the oscilloscope. Whenever it was necessary to isolate a specific spectral transition for PMT measurements, a bandpass interference filter (e.g. Melles Griot 03 FIU 127 for the N_2 (C-B 0-0 transition)) was inserted into the optical path. The experimental set-up is depicted in Fig. 1.

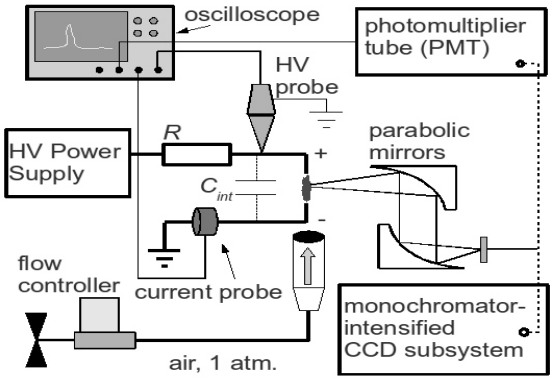

Fig. 1. Schematic of the experimental setup, HV – high voltage, R – resistor.

3. Transient Spark

TS is a filamentary streamer-to-spark transition discharge initiated by a streamer, which transforms to a short spark pulse (Fig. 2) due to the discharge of the capacity (*C*), composed of the internal capacity of the discharge chamber C_{int}, capacity of the HV cable between the resistor *R* and the HV electrode, and capacity of the HV probe. When *C* is discharged, the current given by

$$I(t) \quad C\frac{dU}{dt} \tag{1}$$

reaches a high value (~1 A) and the voltage drops to zero due to the resistive fall on the external resistance *R*. Then, during the quenched phase, *C* is recharged by a growing potential *U* on the stressed electrode.

The potential *U* grows in time *t* according to the following equation:

$$U(t) \quad U_o \quad 1 \quad \exp\ \frac{t}{RC} \tag{2}$$

where U_o is the high voltage applied to the stressed electrode. Usually, during this relaxation phase when the gap potential crosses a specific threshold, there appears a corona dis-

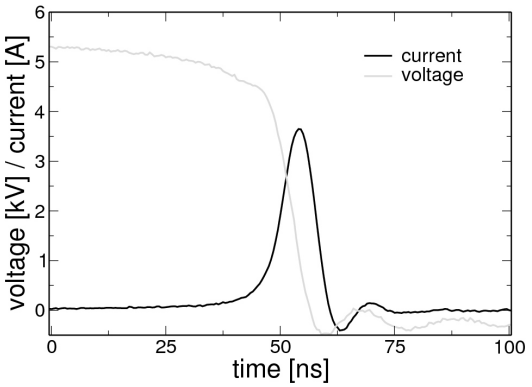

Fig. 2. Typical TS current and voltage waveforms, repetition frequency ~5 kHz, U_o = 10 kV.

charge in its glow regime, and some pre-breakdown streamers. As soon as C is sufficiently charged again, it triggers a new TS pulse. It occurs in time $t \quad T$, at discharge voltage U_{TS} which is given according to the (2) by:

$$U_{TS} \quad U_o \; 1 \quad \exp \; \frac{T}{RC} \tag{3}$$

From the (3) we get the characteristic repetition frequency f of this process:

$$f \quad \frac{1}{T} \quad \frac{1}{RC \ln \; \frac{U_o}{U_o \quad U_{TS}}} . \tag{4}$$

For typical R and C, the repetition frequency f is in order of several kHz. However, the measured frequency is not absolutely regular. The TS breakdown voltage U_{TS} may also depend on f, especially at higher f, when the electrode's gap may remain pre-ionized. Thus, the next TS breakdown occurs at lower U_{TS}. Lower U_{TS} consequently increases f. As f extends a certain value, TS may transform into a pulse-less glow discharge regime with a constant current of few mA. This transition is controlled by the external resistance R, the distance between the electrodes, and the gas flow rate. Both TS and glow discharge regime are described in more detail in [6, 10, 11].

4. Results and discussion

4.1. Electrical characteristics of the discharge

When the high voltage U_o applied to the stressed electrode is progressively increased, we first observe a streamer corona. When the threshold voltage for TS is reached, a transition to TS occurs at the discharge voltage U_{TS}. The repetition frequency of these first TS pulses is low and very irregular (Fig. 3). The further increase of U_o leads to a monotonous increase of f (Fig. 4) and TS pulses become more regular (Fig. 3). However, individual pulses are not identical and U_{TS}, as well as f, vary around their average values.

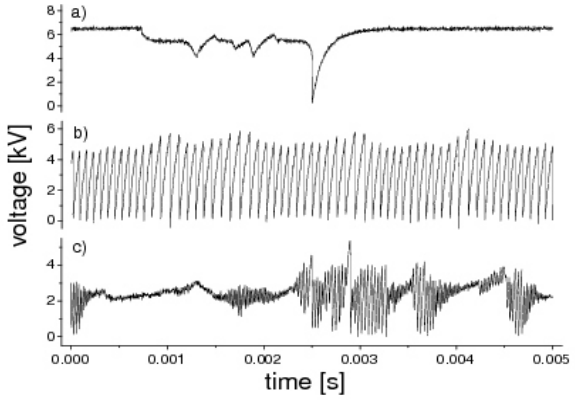

Fig. 3. Voltage waveforms of different discharge regimes: a) the first random TS pulses, b) regular TS, c) unstable glow regime.

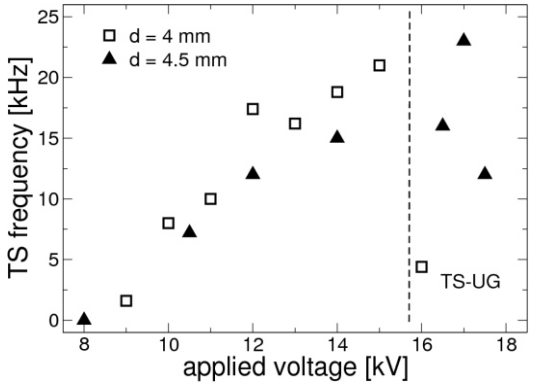

Fig. 4. Discharge frequency as a function of the applied voltage U_o, TS-UG represents the region of the unstable glow regime, experiments with three different electrode's gaps (d).

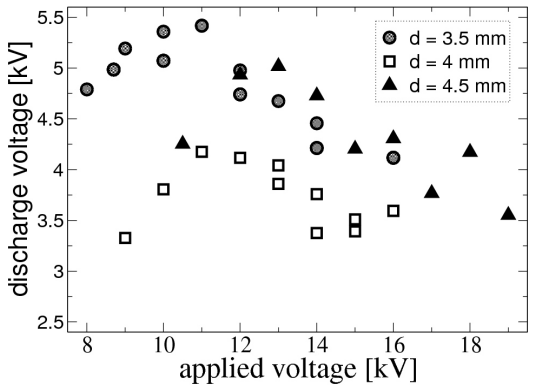

Fig. 5. Discharge voltage U_{TS} as a function of applied voltage U_o.

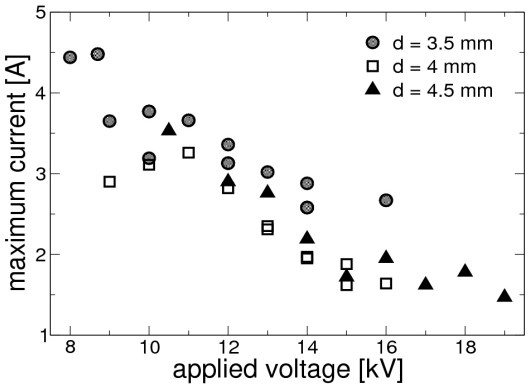

Fig. 6. Maximum current in pulse I_{max} as a function of applied voltage U_o.

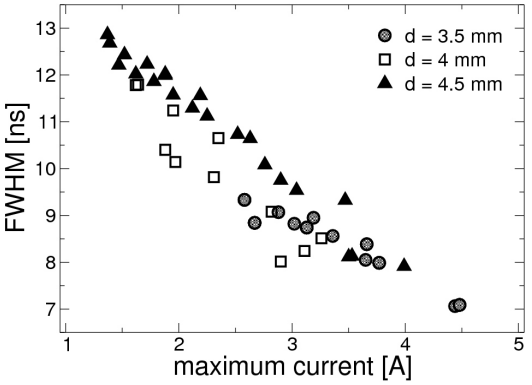

Fig. 7. Full width of the pulse at half maximum (FWHM) as a function of I_{max}.

Figure 5 shows the dependence of the average U_{TS} on U_o. The decrease of U_{dis} for a higher U_o can be explained by the increasing gas temperature in the discharge channel, resulting in a decreasing gas density N. Since some threshold reduced electric field E/N is needed to initiate the TS pulse, E and therefore also U_{TS} may be lowered now.

With the increase of U_o, the maximum pulse current (I_{max}) decreases (Fig. 6) and this decrease is accompanied by the broadening of the pulses (Fig. 7). As a result, no significant dependence of the integrated current per pulse (Q) on U_o is observed, and due to the increasing f the mean discharge current (I_{mean}) increases linearly with U_o. When the frequency exceeds around 20 kHz, the discharge tends to convert to the glow regime. However, due to the high value of R and the electro-negativity of air, this regime is not stable and the discharge randomly switches between the glow regime and the high frequency TS regime (Fig. 3).

TS is based on the charging and discharging of C, the integrated current Q_p and the energy delivered to the discharge gap per pulse (E_p) are therefore functions of U_{dis} and they can be expressed as

$$Q_p \quad CU_{TS} \tag{5}$$

and

$$E_p \quad CU_{TS}^2 / 2, \tag{6}$$

respectively. The knowledge of the value of C is therefore important for the description and characterization of TS. First, we calculated C by fitting the obtained current waveforms with current obtained as the negative derivate of the measured voltage waveforms (Eq. 1). By this way we found C to be 6.3 ± 0.3 pF. The values of Q_p and E_p calculated from Equations (5) and (6), respectively, using this value of C, are in agreement with Q_p and E_p obtained by the integration of $I(t)$ and $U(t).I(t)$ for the whole period of the current pulse. On the other hand, this value of C significantly overestimates the TS repetition frequency calculated from Equation (4).

We therefore calculated the C also from the growth of the voltage on the stressed electrode during the relaxation period (Eq. 2). We obtained another value of C = 14 ± 1 pF, which enables a correct calculation of f. As a result, we have two values of C, the lower one suitable for the description of the discharging event and the second one suitable for the description of the charging period. The understanding of this phenomenon requires further study, but we assume that it can be partially explained by the losses through the HV voltage probe and corona discharge. The used HV probe has its characteristic resistance R_s = 100 M . This resistance is very high if compared with the resistance of the discharge gap during the spark pulse when the gap is bridged by the conductive plasma. Nevertheless, it is higher or comparable with the gap resistance during the relaxation time without spark pulse. During this time when C is charged, there appears a current which escapes through R_s. Additionally, when the threshold voltage for the corona discharge is achieved, the corona current also slows down the charging of C. As a results, these two processes prolong the time required to achieve U_{TS}, and this is related to the apparent increase of C in the Equations (2), (3) and (4).

4.2. Emission study

In the UV-VIS emission spectra of TS, the strongest lines observed can be attributed to the emission of N_2 2nd positive system (C^3 $_u$ – B^3 $_g$) and atomic O line (at 777 nm). Emission of N_2 1st positive system (B^3 $_g$ – A^3), N_2^+ 1st negative system (B^2 – X^2), and atomic N lines is also observed. The presence of N_2^+ and atomic lines indicate that the plasma has a high electron temperature and a significant level of non-equilibrium. Non-equilibrium conditions are also confirmed by a difference between the vibrational (T_v) and rotational (T_r) temperatures obtained by fitting the experimental spectra of N_2 2nd positive system with the simulated ones (using the Specair program [13]). degree of non-equilibrium probably decreases with increasing U_o, because T_r increases from about 500 K to 1 500 K (Fig. 8) and T_v increases from about 3 800 K to 5 000 K (Fig. 9).

The temporal emission profiles (Fig. 8) were obtained using the PMT with either no filter or with bandpass interference filters transparent for radiation around 337 nm and 777 nm for the selection of N_2 2nd positive system and atomic O line emission, respectively. It was found that the maximum intensity of total emission lags from approximately 5 to 15 ns behind the current pulse maximum. This value decreases with

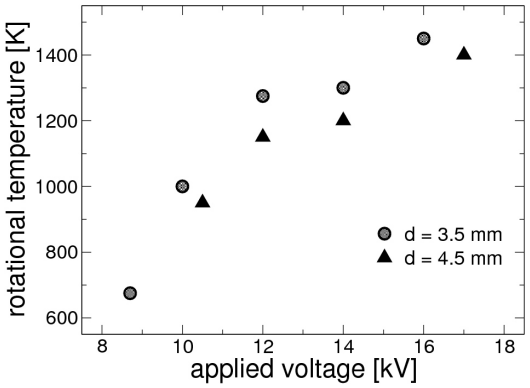

Fig. 8. Rotational temperature measured from N_2 (C-B, 0-0) as a function of U_o.

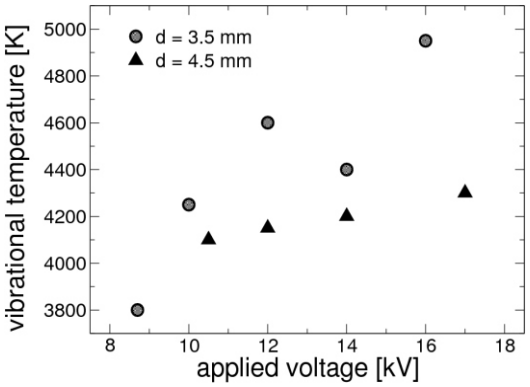

Fig. 9. Vibrational temperature of N_2 (C) species as a function of U_o.

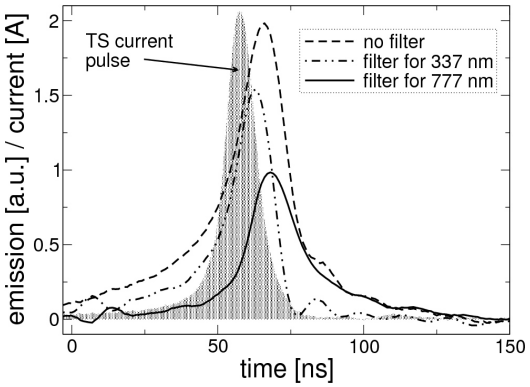

Fig. 10. Normalized temporal emission profiles obtained by PMT with filter for N_2 (C-B, 0-0) (337 nm), filter for O* emission (777 nm), and with no filter.

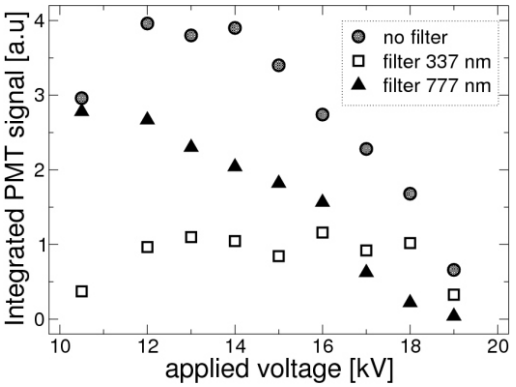

Fig. 11. Integrated emission of N_2 (C-B, 0-0) (filter for 337 nm), O* (filter for 777 nm) and total emission (no filter) per pulse, obtained by PMT as a function of U_o, d = 4.5 mm.

increasing U_o. The maximum of the emission of N_2 2^{nd} positive system precedes the maximum of total emission and emission of atomic O line by about 5 and 8 ns, respectively. The emission of N_2 2^{nd} positive system is also quenched faster, within 20 ns after the current pulse maximum, than the emission of atomic O (Fig. 8), which is quenched within 100 ns after the current pulse maximum. The dependence of integrated intensity of total emission and the emission of N_2 2^{nd} positive system (Fig. 11) on U_o is similar to behavior of U_{TS} as functions of U_o (Fig. 5). Thus, they are proportional to the Q_p. On the other hand, the intensity of atomic O line emission decreases monotonously with U_o. The explanation of all phenomena observed by PMT measurements will require further research, including plasma kinetic modeling.

5. Conclusions

We investigated electrical characteristics and emission spectra of a DC-supplied periodic streamer-to spark transition discharge in atmospheric air, called transient spark (TS). Thanks to the very short spark pulse duration given by the small internal capacity of the discharge chamber and a limiting series resistor, the plasma generated by TS cannot reach the LTE conditions. The periodic streamer-to-spark transition provides non-equilibrium conditions with fast electrons resulting in strong chemical effects. The existence of non-equilibrium conditions is also confirmed by the inferred vibrational and rotational temperatures.

TS in air generates N_2 excited species, N and O atoms, and N_2^+ ions. The low frequency mode with stronger and shorter current pulses apparently generates higher concentrations of radicals per pulse. However, due to increasing average repetition frequency, the regime with pulses of average amplitude and repetition frequency around 10 kHz, where the strongest emission of N_2 2^{nd} positive system was observed, seems the most suitable for the chemical effects.

Acknowledgements

This work was carried out under the support of APVV 0267-06, VEGA 1/0293/08, and EOARD FA8655-08-1-3061 grants.

References

[1] L. Civitano: Non-Thermal Plasma Techniques for Pollution Control, eds. B. Penetrante, S. E. Schultheis (Springer, New York, 1993) NATO Series, Vol. 1, p. 103.
[2] A. A. Joshi, B. R. Locke, P. Arce, W. C. Finney: Journal of Hazardous Materials, **41** (1995) 3.
[3] M. Laroussi: IEEE Trans. Plasma Sci. **30** (2002) 1409.
[4] M. Cernak, J. Rahel, D. Kovacik, M. Simor, A. Brablec, P. Slavicek: Contrib. Plasma Phys. **44** (2004) 492.
[5] J. Pawlat, K. Hensel, S. Ihara: Acta Phys. Slovaca **55** (2005) 479.
[6] Z. Machala, M. Janda, K. Hensel, I. Jedlovsky, L. Lestinska, V. Foltin, V. Martisovits, M. Morvová: J. Mol. Spectrosc. **243** (2007) 194.
[7] D. Pai, D. A. Lacoste, C. O. Laux: IEEE Trans. Plasma Sci. **36** (2008) 974.
[8] C. O. Laux, T. G. Spence, C. H. Kruger, R. N. Zare: Plasma Sources Sci. Technol. **12** (2003) 125.
[9] U. Fantz: Plasma Sources Sci. Technol. **15**, S137 (2006).
[10] Z. Machala, I. Jedlovsky, V. Martisovits: IEEE Trans. Plasma Sci. **36** (2008) 918.
[11] Z. Machala, E. Marode, C. O. Laux, C. H. Kruger: J. Adv. Oxid. Technol. **7** (2004) 133.
[12] C. O. Laux: Radiation and Nonequilibrium Collisional-Radiative Models, von Karman Institute for Fluid Dynamics, Lecture Series 2002-07, Rhode Saint-Genese, Belgium, 2002.